Distribution of ubiquilin 2 and TDP-43 aggregates throughout the CNS in *UBQLN2* p.T487I-linked amyotrophic lateral sclerosis and frontotemporal dementia

Laura R. Nementzik[1,2], Kyrah M. Thumbadoo[1,2], Helen C. Murray[2,3], David Gordon[1,2], Shu Yang[4], Ian P. Blair[4], Clinton Turner[2,3,5], Richard L. M. Faull[2,3], Maurice A. Curtis[2,3], Catriona McLean[6], Garth A. Nicholson[4,7,8], Molly E. V. Swanson[1,2], Emma L. Scotter[1,2]

1 School of Biological Sciences, University of Auckland, Auckland, New Zealand.
2 Centre for Brain Research, University of Auckland, Auckland, New Zealand.
3 Department of Anatomy and Medical Imaging, University of Auckland, Auckland, New Zealand.
4 Centre for Motor Neuron Disease Research, Department of Biomedical Sciences, Faculty of Medicine, Health, and Human Sciences, Macquarie University, North Ryde, NSW, Australia.
5 Department of Anatomical Pathology, LabPlus, Auckland City Hospital, Auckland, New Zealand.
6 Department of Anatomical Pathology, Alfred Health, Melbourne, VIC, Australia.
7 Northcott Neuroscience Laboratory, ANZAC Research Institute, Sydney, Australia.
8 Molecular Medicine Laboratory, Concord Repatriation General Hospital, Sydney, Australia.

Corresponding author:
Email, emma.scotter@auckland.ac.nz; Telephone, +64 9 923 1350

Acknowledgements and funding

This publication is dedicated to the incredible patients and families who contribute to our research. We thank Marika Eszes at the Centre for Brain Research, University of Auckland, New Zealand, and the Neurological Foundation of New Zealand for their ongoing financial support of the Human Brain Bank. We also thank Fairlie Hinton at the Victorian Brain Bank, which is supported by The Florey, The Alfred, Victorian Institute

of Forensic Medicine and Coroners Court of Victoria and funded in part by Fight Parkinson's, MND Victoria, FightMND, Yulgilbar Foundation and Ian and Maria Cootes. The imaging data reported in this paper were obtained at the Biomedical Imaging Research Unit, operated by the Faculty of Medical and Health Sciences' Technical Services at the University of Auckland. KT was supported by a doctoral scholarship from Amelia Pais-Rodriguez and Marcus Gerbich. HCM was supported by a Health Education Trust Postdoctoral Fellowship. ELS was supported by Marsden FastStart and Rutherford Discovery Fellowship funding from the Royal Society of New Zealand [15-UOA-157, 15-UOA-003]. This work was also supported by grants from Motor Neuron Disease NZ, Freemasons Foundation of New Zealand, Matteo de Nora, and PaR NZ Golfing. No funding body played any role in the design of the study, nor in the collection, analysis, or interpretation of data nor in writing the manuscript.

Authors' contributions

LRN, KMT, BVD, HCM, MEVS conducted or designed experiments; LRN, MEVS performed data analysis and designed analysis methods; CT and CM conducted neuropathological diagnostics; SY, IPB, RLMF, MAC, FH, GAN coordinated the banking and use of human tissue for study; LRN, KMT, MEVS, ELS wrote the manuscript; ELS conceived of and designed the study. All authors read, edited, and approved the final manuscript.

Abstract

Mutations in the *UBQLN2* gene cause amyotrophic lateral sclerosis (ALS) and frontotemporal dementia (FTD). The neuropathology of such *UBQLN2*-linked cases of ALS/FTD is characterised by aggregates of the ubiquilin 2 protein in addition to aggregates of the transactive response DNA-binding protein of 43 kDa (TDP-43). ALS and FTD without *UBQLN2* mutations are also characterised by TDP-43 aggregates, that may or may not colocalise with wildtype ubiquilin 2. Despite this, the relative contributions of TDP-43 and ubiquilin 2 to disease pathogenesis remain largely under-characterised, as does their relative deposition as aggregates across the central nervous system (CNS). Here we conducted multiplex immunohistochemistry of three *UBQLN2* p.T487I-linked ALS/FTD cases, three non-*UBQLN2*-linked (sporadic) ALS cases, and eight non-neurodegenerative disease controls, covering 40 CNS regions. We then quantified ubiquilin 2 aggregates, TDP-43 aggregates, and aggregates containing both proteins in regions of interest to determine how *UBQLN2*-linked and non-*UBQLN2*-linked proteinopathy differ. We find that ubiquilin 2 aggregates that are negative for TDP-43 are predominantly small and punctate, and are abundant in the hippocampal formation, spinal cord, all tested regions of neocortex, medulla, and substantia nigra in *UBQLN2*-linked ALS/FTD but not sporadic ALS. Curiously, the striatum harboured small punctate ubiquilin 2 aggregates in all cases examined, while large diffuse striatal ubiquilin 2 aggregates were specific to *UBQLN2*-linked ALS/FTD. While ubiquilin 2 deposition in frontotemporal regions may enhance cognitive risk in *UBQLN2*-linked cases, ubiquilin 2 is deposited mainly in clinically unaffected regions throughout the CNS such that overall symptomology in these cases maps best to the aggregation of TDP-43.

Keywords: *UBQLN2*, ubiquilin 2, amyotrophic lateral sclerosis (ALS), frontotemporal dementia (FTD), neuropathology, human, TDP-43

Introduction

A key pathological feature of amyotrophic lateral sclerosis (ALS) and frontotemporal dementia (FTD), present in 97% of ALS cases regardless of aetiology, is neuronal and oligodendrocytic aggregates of the TAR DNA binding protein of 43 kDa (TDP-43) [1-3]. In ALS caused by penetrant dominant genetic mutations, brain and/or spinal tissue often contains aggregates of both TDP-43 and the mutant-gene-encoded protein [4, 5]. Yet it is TDP-43 aggregate burden that correlates with neurodegeneration in sporadic ALS [6-8], and in *C9orf72*-linked ALS/FTD, which is characterised by additional deposition of dipeptide repeat proteins (DPRs) [9]. Whether the distribution of pathological TDP-43, or rather the mutant-gene-encoded protein, underpins clinical phenotype in cases with rarer genotypes is unknown. Mutations in *UBQLN2* cause X-linked dominant ALS with or without FTD [4]. *UBQLN2*-linked cases show deposition of TDP-43 and ubiquilin 2 aggregates in several CNS regions but these have not been mapped extensively, nor with respect to one another [4, 10-13].

Ubiquilin 2 is a ubiquitin-binding protein that delivers ubiquitinated substrates to the 26S proteasome for degradation [14, 15]. It also functions in autophagy, co-localising with LC3-II and optineurin in autophagosomes [16, 17], and regulating autophagosme acidification via the vacuolar ATPase proton pump [18]. Under cellular stress, and if not ubiquitin-bound, ubiquilin 2 undergoes liquid-liquid phase separation and is recruited to cytoplasmic stress granules [19]. The majority of ALS-causing mutations in ubiquilin 2 occur in or near a proline-rich repeat domain [4, 10, 12, 20-22], altering ubiquilin 2 phase separation dynamics, promoting liquid-to-solid transitions and, for certain mutants, driving ubiquilin 2 itself to aggregate [23]. Mutations in ubiquilin 2 also impair proteasome and/or autophagy function, thus promoting accumulation and aggregation of their degradation substrates including TDP-43 [4, 24, 25].

TDP-43 is a DNA- and RNA-binding protein with diverse roles in DNA maintenance and RNA processing; regulating DNA repair, mRNA stability and splicing, microRNA biogenesis and more [26, 27]. In most ALS cases, TDP-43 is found deposited in *post-*

mortem brain and spinal cord tissue as neuronal and oligodendrocytic aggregates [1, 2, 28], predominantly in the motor cortex, spinal cord ventral horn, and cranial nerve nuclei [6]. Further 'spreading' of aggregates in ALS involves synaptically connected cortical and midbrain regions, with deposition of TDP-43 aggregates in the temporal lobe and hippocampus seen selectively in cases with abundant and distributed TDP-43 pathology ("stage 4") [6].

Investigation of ubiquilin 2 and TDP-43 pathology in *UBQLN2*-linked ALS/FTD tissue has been limited, with ubiquilin 2-positive aggregates having only been identified in the hippocampus, spinal cord, neocortex, and brainstem [4, 10, 12, 13, 20, 29] (Fig. 1). In *UBQLN2*-linked ALS/FTD spinal cord, ubiquilin 2 aggregates have been shown to colocalise with TDP-43, however the same is also true of most non-*UBQLN2*-linked ALS/FTD [4, 12]. Our group recently showed that ubiquilin 2 in the hippocampus in *UBQLN2*-linked cases is more aggregation-prone than in non-*UBQLN2*-linked cases, with mutant but not wildtype ubiquilin 2 often aggregating independently of a known scaffold [13]. However, in other CNS regions in *UBQLN2*-linked disease, it is unclear whether ubiquilin 2 aggregation occurs together with TDP-43 or independently of a TDP-43 'scaffold'.

A large multigenerational family with members in New Zealand, Australia, and the United Kingdom shows a c.1460C>T mutation in *UBQLN2*, encoding a threonine to isoleucine amino acid change (p.T487I), that co-segregates with ALS with or without FTD [12]. Donated brain and spinal cord tissue was available from three affected members of this family, each harbouring the p.T487I *UBQLN2* mutation. Here we employ multiplex immunohistochemistry to map ubiquilin 2 and TDP-43 aggregates across the CNS in these individuals, compared to controls and stage 4 sporadic ALS (sALS). We seek to characterise the differential aggregation propensities of mutant and wildtype ubiquilin 2 across the CNS, and to identify the CNS regions in which ubiquilin 2 aggregation occurs independently of TDP-43, to enable clinicopathological correlation and targeting of the true molecular 'driver' of pathogenesis.

Materials and methods

Systematic review of ubiquilin 2 and TDP-43 pathology in *UBQLN2*-linked ALS CNS tissue from published studies.

Journal articles were identified using PubMed that performed immunohistochemical staining for ubiquilin 2 and/or TDP-43 in post-mortem ALS/FTD human brain tissue from cases with a *UBQLN2* mutation. Those that were not primary research articles or not published in English were excluded. Seven papers were identified from which neuropathological data for ubiquilin 2 and TDP-43 were extracted and tabulated (Figure 1).

Patient demographics and CNS tissue

Formalin-fixed paraffin-embedded (FFPE) post-mortem brain tissue was obtained from eight neurologically normal control cases, three sporadic ALS (sALS) cases with phosphorylated TDP-43 proteinopathy (pTDP-43) classified as 'stage 4' [6], and three related *UBQLN2* p.T487I-linked familial ALS cases with or without FTD. Patient demographic and clinical information is summarised in Table S1. Tissue was obtained from up to 40 subregions of each brain, within the hippocampal formation and associated cortices, spinal cord, neocortex, striatum, medulla, substantia nigra, and cerebellum (Table S2). Tissue from all controls and sALS cases, and *UBQLN2*-linked case ALS+FTD MN17, was obtained from the Neurological Foundation Human Brain Bank at the Centre for Brain Research, Auckland, New Zealand, and processed as previously described [30]. It should be noted that the latter (MN17) was stored in fixative for 7 years before embedding. All NZ cases, but no controls, had confirmed pTDP-43 proteinopathy in the motor cortex. Tissue from two other *UBQLN2* p.T487I-linked cases were obtained from: the Victoria Brain Bank (pedigree ID V:7 in Figure 1A of [12], with ALS+FTD); and the Centre for Motor Neuron Disease Research, Macquarie University (pedigree ID IV:10 in Figure 1A of [12], with ALS). Clinical and neuropathological diagnoses were conducted as described previously [12, 29] or by the Victoria Brain Bank for case V:7 (diagnosis not previously described).

Multiplexed fluorescent immunohistochemistry

Fluorescence immunohistochemistry was performed as described previously [31, 32]. Briefly, tissue sections were cut with a microtome in the transverse plane at a thickness of 7 µm and mounted onto ÜberFrost® Printer Slides (InstrumeC). Mounted sections were dried at room temperature or at 37 °C before immunohistochemistry. Slides were heated to 60 °C for 1 h on a hot plate, then dewaxed and rehydrated through a xylene-alcohol-water series: 100% xylene, 2x 30 min; 100% ethanol, 2x 15 min; 95%, 85%, 75% ethanol, 5 min each; water 3x 5 min. Antigens were retrieved through immersion in 10 mM sodium citrate buffer (0.05% Tween 20, pH 6.0) in a pressure cooker (Retriever 2100, Electron Microscopy Sciences) at 120 °C for 20 min and cooled to room temperature for 100 min. Sections were washed 3x for 5 min in 1x phosphate-buffered saline (PBS) or distilled water, and wax borders were drawn with an ImmEdge Hydrophobic Barrier PAP pen. Sections were permeabilised in PBS-T (PBS with 0.2% Triton™ X100) for 15 min at 4 °C, followed by 3x 5-min PBS washes. Lipofuscin autofluorescence was quenched using TrueBlack® Lipofuscin quencher (Biotium) 1:20 in 70% ethanol for at least 30 seconds followed by three vigorous water washes. Sections were blocked with 10% normal goat serum (Thermo Fisher Scientific) in PBS for 1 h, then incubated at 4 °C overnight with primary antibodies (Table S3). *UBQLN2*-linked ALS+FTD case V:7 showed poor Hoechst labelling of nuclei, therefore a primary antibody against histone H3 was used as a nuclear marker instead for this case. To aid detection of TDP-43 aggregates by quantitative analysis, we pooled pan- and phospho-TDP-43 antibodies (both rat IgG2a, identified only as ‘TDP-43’). Following PBS washes, species- and isotype-specific secondary antibodies and Hoechst 33342 nuclear stain (Table S4) were applied for 3 h in 1% normal goat serum at room temperature. After final 3x 5-min PBS washes, sections were coverslipped with #1.5 coverslips (Menzel-Gläser) using ProLong® Gold Antifade Mountant (Thermo Fisher Scientific). Bleed-through (Fig. S1), secondaries-only, and neurologically normal control sections were included for each staining.

Cross-reactivity was observed during staining optimisation, between goat anti-mouse IgG1 secondary antibodies and rat IgG2a primary antibodies. Therefore, for quantitative

analysis of spinal cord and motor cortex sections which required labelling with both SMI-32 (mouse IgG1) and pooled pan- and phospho-TDP-43 antibodies (both rat IgG2a), two sequential rounds of immunofluorescent labelling were performed as shown in Table S3. Following first-round imaging, coverslips were removed by soaking slides in PBS overnight, and first-round antibody staining was eliminated using NewBlot™ IR Stripping Buffer 5X (Licor) for approximately 13 minutes. Washing, permeabilization, and blocking steps were repeated as described above and a second round of primary and secondary antibody staining was performed on the same tissue sections, for SMI-32 and a nuclear marker, before re-imaging. First- and second-round images were spatially aligned as described previously [32].

Image acquisition

Wide-field images for qualitative or quantitative analysis were acquired using a Zeiss Z2 Axioimager with a MetaSystems VSlide slide scanning microscope (20x dry magnification lens, 0.9 NA) with a Colibri 7 solid-state fluorescent light source. Single filters, as described and validated previously [33], were used to excite fluorophores and detect the following wavelengths (Ex peak/range (nm); Em peak/range (nm)): Filter set #1 (385/30; 447/60), #3 (469/38; 527/20), #4 (555/30; 580/23), #5 (590/27; 628/32), #6 (631/33; 676/29), and #7 (735/40; 809/81) and visualised with MetaFer software (MetaSystems, v.3.12.1) equipped with a CoolCube 4m TEC (monochrome) sCMOS digital camera. Image tiles were stitched using MetaCyte software, and stitched images were extracted using VSViewer software (MetaSystems, v.1.1.106). Exposure times for each channel were set per case due to differences in immunoreactivity between control, sALS cases, and *UBQLN2*-linked ALS+FTD cases. *UBQLN2*-linked ALS+FTD case MN17 showed poor immunoreactivity overall, likely due to long-term fixation, therefore longer exposures were used.

Confocal images were acquired using an Olympus FV1000 confocal microscope (100x magnification oil immersion lens, 1.4 NA, *Z*-step 0.4-1 µm) with FluoView 4.2 software (Olympus). Maximum intensity *Z*-projections were generated and processed using FIJI.

Final figures were compiled using FIJI software (v1.53c, National Institutes of Health) and Adobe Illustrator (Adobe Systems Incorporated, v24.3). Extracted single-channel images were imported into FIJI, merged, and pseudocoloured. For each channel, image intensity was adjusted in FIJI to best view the marker of interest, reduce background autofluorescence, and generate images representative of ubiquilin 2 and TDP-43 aggregate burden in each region.

Qualitative analysis of ubiquilin 2 aggregates

To qualitatively assess which CNS regions showed ubiquilin 2 deposition independent of TDP-43, imaged sections were viewed using VSViewer (v2.1.112, MetaSystems) and assessed for the abundance of ubiquilin 2-only (pTDP-43-negative) aggregates. Anatomical regions and sub-regions were delineated by anatomical markers as follows and as per Table S3: All sub-regions by MAP2; cortical layers and ventral horn motor neurons by SMI-32 [34, 35]; cerebellar cortical layers and dentate nucleus by calbindin [36, 37]; and globus pallidus externa, interna, and putamen by enkephalin [38, 39]. To account for the presence of fluorescent artefacts which only resemble punctate ubiquilin 2 aggregates, ubiquilin 2-only aggregates were considered a consistent pathological feature of a subregion when five or more aggregates were identified in that subregion.

Quantitative analysis of ubiquilin 2-only, TDP-43-only, and ubiquilin 2/TDP-43 double immunopositive aggregates

Image analysis methods to quantify relative ubiquilin 2 and TDP-43 aggregate deposition were developed in MetaMorph v7.10.5.476 (Molecular Devices), similar to those previously described [8, 40]. Antibodies panels used are given in Table S3. Briefly, a composite image of MAP2 and Hoechst for each section was used to identify and retain each subregion of interest and exclude tissue folds and defects. Nuclear TDP-43 (only detected in stage 4 sALS) was excluded by using the Count Nuclei application to segment all Hoechst-positive nuclei and removing the nuclear area from the TDP-43 image. Ubiquilin 2 and TDP-43 aggregates were then segmented using absolute thresholding by labelling intensity, excluding single positive pixels, and binary masks created. Ubiquilin 2 and TDP-43 aggregate binary masks were combined to create a ‘master mask’, within

which each object was considered a single aggregate. Aggregates were then phenotyped by measuring the maximum intensity of ubiquilin 2 and TDP-43 immunoreactivity and classifying the aggregate to be ubiquilin 2 or TDP-43 positive if the maximum intensity was greater than the respective threshold used in the initial segmentation. This identified 3 aggregate populations: ubiquilin 2-only, TDP-43-only, and ubiquilin 2- and TDP-43-double-immunopositive. The densities of each aggregate type were determined by normalising aggregate number to the subregion area. For ubiquilin 2- and TDP-43-double-immunopositive aggregates, the number of double-immunopositive aggregates was normalised to 1) total aggregates identified, 2) total ubiquilin 2-positive aggregates identified, and 3) total TDP-43-positive aggregates identified.

It should be noted that thresholds for segmenting aggregates and classifying them as positive were optimised separately for each case, due to variability in tissue fixation and antigenicity, but kept consistent between regions within a case. This quantification should therefore be used to compare aggregate deposition across the CNS within a case, rather than to compare between cases.

Results

Ubiquilin 2 and TDP-43 labelling in previous studies largely fails to discriminate between their independent aggregation and co-aggregation

Review of the literature describing ubiquilin 2 and TDP-43 neuropathology in *UBQLN2*-linked human ALS/FTD identified 7 results, as summarised in Figure 1. Ubiquilin 2 neuropathology had been reported in the hippocampus, spinal cord, inferior olivary nucleus, and neocortex. TDP-43 neuropathology had been reported in the hippocampus, spinal cord, motor cortex, neocortex, amygdala, putamen, thalamus, and hypoglossal nucleus. Only in hippocampus and spinal cord had co-immunolabelling been performed for ubiquilin 2 and TDP-43, including by us. Co-immunolabelling indicated that in hippocampus, mutant ubiquilin 2 aggregates either independently of TDP-43 (molecular layer [4, 13]) or co-aggregates with TDP-43 (granule cell layer [10, 13]), and in spinal cord, mutant ubiquilin 2 co-aggregates with TDP-43 [4, 12]. For other brain regions, the relationship between ubiquilin 2 and TDP-43 aggregation was unknown.

Ubiquilin 2-only aggregates are seen across much of the CNS in *UBQLN2* p.T487I-linked ALS/FTD

To compare the distribution of aggregates of ubiquilin 2 with TDP-43 across the CNS, we compared tissue from 1-3 *UBQLN2* p.T487I-linked ALS/FTD cases with tissue from two stage 4 sALS cases and two non-neurodegenerative disease controls, from up to 40 CNS subregions (Table S2). We first identified aggregates that were positive for ubiquilin 2 and negative for TDP-43 (ubiquilin 2-only aggregates). Strikingly, these ubiquilin 2-only aggregates comprised the vast majority of all ubiquilin 2 aggregates in *UBQLN2* p.T487I-linked ALS/FTD. They were clearly present (>5 aggregates per sub-region) in the following subregions: every neocortical subregion; cervical, thoracic, and lumbar levels of the spinal cord; the dentate gyrus of the hippocampus (see also [13]); the subiculum, entorhinal cortex, and perirhinal cortex of the parahippocampus; most subregions of the medulla; the putamen, the ventral striatum, and the caudate nucleus. Ubiquilin 2-only aggregates were scarce in or absent from *UBQLN2* p.T487I-linked

ALS/FTD cases in the pyramids, raphe nuclei, and medial lemniscus of the medulla; the globus pallidus; and the cerebellum.

Confocal microscopy of aggregate morphology showed that ubiquilin 2 aggregates in *UBQLN2* p.T487I-linked ALS/FTD cases were small and punctate in almost all CNS subregions (Fig. 2A_1, showing caudate nucleus, punctate aggregates appearing ~2-3 µm). Larger diffuse ubiquilin 2 aggregates were rare, being seen mainly in the neocortex, the parahippocampus, and being most abundant in the striatum (Fig. 2A_2, appearing ~10 µm). These large diffuse aggregates were occasionally perinuclear (Fig. 2A_2'), while punctate aggregates were neuritic or found in the neuropil. Unexpectedly given previous literature, spinal cord lower motor neuron TDP-43 aggregates were ubiquilin 2-negative in both *UBQLN2* p.T487I-linked ALS/FTD and stage 4 sALS (Figs. 2B, C). However, punctate ubiquilin 2-only aggregates were present in the spinal cord dorsal horn and motor cortex in *UBQLN2* p.T487I-linked ALS/FTD cases (Fig. 2D, F) while smaller dot-like ubiquilin 2-only aggregates were present in the spinal cord dorsal horn and motor cortex in stage 4 sALS cases (Fig. 2E, G). Overall, ubiquilin 2-only aggregates appeared to be abundant throughout most of the CNS in *UBQLN2* p.T487I-linked ALS/FTD.

Ubiquilin 2-only aggregates, but not TDP-43-only aggregates, are abundant in *UBQLN2* p.T487I-linked ALS/FTD hippocampal formation, and entorhinal and perirhinal cortices

Having qualitatively identified CNS regions in *UBQLN2* p.T487I-linked ALS/FTD with deposition of ubiquilin 2-only aggregates, and examined their morphology, we next conducted automated quantitative analysis. Subregions of the hippocampal formation and associated cortices, spinal cord, motor cortex (representing the neocortex), and striatum were analysed in 2-3 *UBQLN2* p.T487I-linked linked ALS/FTD cases compared to 3 stage 4 sALS cases, for ubiquilin 2-only, TDP-43-only, and ubiquilin 2- and TDP-43-double-immunopositive aggregates. As noted, the middle and lower medulla and substantia nigra also contained ubiquilin-2 only aggregates, but these were not quantified (Figs. S2-4).

In the hippocampal formation, ubiquilin 2-only aggregates in *UBQLN2* p.T487I-linked ALS/FTD were found in the molecular layer (Fig. $3A_1$, B_1, K; 31-314 aggregates/ mm^2), subiculum (Fig. 3E, F, K; 79-13,041 aggregates/ mm^2), entorhinal cortex (Fig. 3G, H, K; 72-425 aggregates/ mm^2), and perirhinal cortex (Fig. 3I, J, K; 335-771 aggregates/ mm^2). As we have shown previously [13], ubiquilin 2-only aggregates in *UBQLN2* p.T487I-linked ALS/FTD were rare in or absent from the granule cell layer (Fig. $3A_2$ (absent), B_2 (absent), K) or cornu ammonis (Fig. 3C, D, K). Ubiquilin 2-only aggregates in stage 4 sALS were generally absent from the hippocampal formation and associated cortices (Figs. S6A-O), with their highest density being in the perirhinal cortex of case MN13 where they were primarily dot-like (Fig. 3L and S6M-M'; 33 aggregates/ mm^2). Occasionally, larger ubiquilin 2 aggregates that colocalised with TDP-43 were found in stage 4 ALS (Fig. S5D).

In contrast, TDP-43-only aggregates in *UBQLN2* p.T487I-linked ALS/FTD were found throughout the hippocampus at low density (Fig. $3B_2$", C", G"-J", K; 0-10 aggregates/ mm^2), and in the subiculum at moderate density (Fig. 3F", K; 17-271 aggregates/ mm^2). TDP-43-only aggregates in stage 4 sALS were also found throughout the hippocampus and subiculum (Fig. 3L and S6D-O") and were particularly abundant in the granule cell layer (Fig. 3L and $S6A_2$", B_2", C_2"; 205-3077 aggregates/ mm^2), as reported previously [6]. Overall, hippocampal ubiquilin 2-only aggregates were predominantly seen in *UBQLN2* p.T487I cases, and TDP-43-only aggregates in stage 4 sALS cases, and with a lack of regional relationship between aggregates of the two proteins.

Ubiquilin 2-only aggregates are abundant in *UBQLN2* p.T487I-linked ALS/FTD dorsal horn, but not ventral horn, of the spinal cord

In the spinal cord, ubiquilin 2-only aggregates were found almost exclusively in the dorsal grey matter (DGM, particularly layer II) in both *UBQLN2* p.T487I-linked ALS/FTD in which they were abundant (Fig. 4A-C_1", G; 5-141 aggregates/ mm^2), and stage 4 sALS in which they were scarce (Fig. 4H, 0-17 aggregates/ mm^2). This was true for cervical, thoracic, and lumbar segments of the cord. Ubiquilin 2-only aggregates were

rare in or absent from the white matter or ventral grey matter in both *UBQLN2* p.T487I-linked ALS/FTD (Fig. 4D-F_1", G) and stage 4 sALS (Figs. S7D-F_1", 4H).

In contrast, TDP-43-only aggregates were found predominantly in the ventral grey matter (VGM) in both *UBQLN2* p.T487I-linked ALS/FTD (Fig. 4D-F_1", G; 3-126 aggregates/ mm^2), and stage 4 sALS (Fig. S7D-F_1", 4H; 31-215 aggregates/ mm^2). This was true for cervical, thoracic and lumbar segments of the cord. TDP-43-only aggregates were rare in or absent from the white matter and dorsal grey matter in both *UBQLN2* p.T487I-linked ALS/FTD (Fig. 4D-F_1", G) and stage 4 sALS (Fig. S7D-F_1", 4H). In contrast to previous findings in *UBQLN2*-linked ALS/FTD and sALS [4, 12], TDP-43 aggregates in the spinal cord did not co-label with ubiquilin 2 in any case. To confirm that this discrepancy was not due to differences in antibody affinity, we labelled spinal cord sections of representative cases of *UBQLN2*-linked ALS/FTD (V:7) and stage 4 sALS (MN30) with a different monoclonal anti-ubiquilin 2 antibody. We still observed ubiquilin 2 puncta in the dorsal horns (Fig. S8A, C), however no colocalization of ubiquilin 2 with TDP-43 aggregates was seen in ventral horn motor neurons (Fig. S8B, D). Overall, spinal cord ubiquilin 2-only aggregates were predominantly found in *UBQLN2* p.T487I cases dorsally, but TDP-43-only aggregates were seen in both *UBQLN2* p.T487I and stage 4 sALS cases ventrally. Again, there was a lack of regional relationship between aggregates of the two proteins.

Ubiquilin 2-only aggregates in *UBQLN2* p.T487I-linked ALS/FTD are abundant throughout the motor cortex

In the motor cortex, ubiquilin 2-only aggregates in *UBQLN2* p.T487I-linked ALS/FTD were found throughout the cortical layers, being particularly abundant in layer VI (Fig. $5A_4$, B_4, C_4; 541-1634 aggregates/ mm^2). Ubiquilin 2-only aggregates in stage 4 sALS were rare or absent from the entire motor cortex, with their highest density being in layers I/II of case MN30 (Fig. 5E; 13 aggregates/ mm^2).

TDP-43-only aggregates in *UBQLN2* p.T487I-linked ALS/FTD were also found throughout the cortical layers, but at lower density than ubiquilin 2 (Fig. 5A-C_5, D; 0-261

aggregates/ mm^2), and mostly driven by ALS case IV:10 (Fig. 5C, D). TDP-43-only aggregates in stage 4 sALS were found throughout the cortical layers (Fig. 5E and S9A-C_5; 14-3762 aggregates/ mm^2) with their highest density being in layers I/II of case MN15 (Fig. 5E and S9B_1; 3762 aggregates/ mm^2). As seen in hippocampus *and* spinal cord, motor cortex ubiquilin 2-only aggregates were predominantly seen in *UBQLN2* p.T487I cases, while, as seen in hippocampus, TDP-43-only aggregates were predominantly seen in stage 4 sALS cases, with a lack of regional relationship.

Ubiquilin 2-only aggregates in *UBQLN2 p.*T487I-linked ALS/FTD are abundant throughout the striatum and can also be found in stage 4 sALS striatum

In the striatum, ubiquilin 2-only aggregates in *UBQLN2* p.T487I-linked ALS/FTD were detected throughout the caudate nucleus, putamen, and ventral striatum, however it should be noted that tissue was only available for 1-2 cases (Fig. 6A-E_2, F; 108-649 aggregates/ mm^2). In addition to the small punctate ubiquilin 2-only aggregates also described in other regions of the CNS (Fig. 6B_1, E_1 arrowheads), larger diffuse ubiquilin 2-only aggregates (Fig. 6B_1, E_1 arrows, appearing ~10 µm) were unique to the striatum. Ubiquilin 2-only aggregates in stage 4 sALS were rare but present in cases MN13 and MN15 (Fig. S10A, B) and more abundant in case MN30 (Fig. 6G and S10C; 108-135 aggregates/ mm^2). When ubiquilin 2 aggregates were found in stage 4 sALS striatum, they occasionally co-labelled with TDP-43 (Fig. S5D).

TDP-43-only aggregates were moderately abundant in striatum in *UBQLN2* p.T487I-linked FTD case V:7 but less so in MN17 (Fig. 6A_2-E_2, F; 10-115 aggregates/ mm^2). TDP-43-only aggregates in stage 4 sALS were abundant in FTD case MN15 (Fig. 6G and S10B-B”$_2$; 1526-4748 aggregates/ mm^2) and present at low to medium density in sALS cases MN13 and MN30 (Fig. 6G and S10A-A_2”, C-C_2”; 4-340 aggregates/ mm^2). Overall, the striatum showed highly variable pathology but emerged as a region with unique large and diffuse inclusions of ubiquilin 2 in *UBQLN2* p.T487I-linked cases. Striatum was also the only brain region with substantial deposition of ubiquilin 2-only aggregates in a stage 4 sALS case, albeit mainly one case.

Ubiquilin 2- and TDP-43-double immunopositive aggregates are differentially distributed in the CNS between *UBQLN2 p.*T487I-linked ALS/FTD and stage 4 sALS

As described in results above, we examined aggregates 'double immunopositive' for ubiquilin 2 and TDP-43 (Fig. S5). Double-immunopositive aggregates in a given case were always rare as a proportion of total aggregates, achieving their highest proportions in *UBQLN2* p.T487I-linked cases in the striatum (up to ~4% of total aggregates, mainly of the large diffuse kind unique to striatum) (Fig. S5C). Double-immunopositive aggregates accounted for a high proportion (up to ~70%) in the hippocampus, and a lower but notable proportion (up to ~25%) in the striatum, of the total (rare) ubiquilin 2 aggregates of sALS cases (Fig. S5D), suggesting that TDP-43 can occasionally drive wildtype ubiquilin 2 aggregation in sALS. Conversely, very few of the (abundant) total ubiquilin 2 aggregates in *UBQLN2* p.T487I-linked cases were TDP-43 positive, as already noted (Fig. S2D). Conversely, approximately one third of the total (rare) TDP-43 aggregates were ubiquilin 2 positive (Fig. S5E), together suggesting that mutant ubiquilin 2 is intrinsically aggregation-prone and does not require, yet may seed, TDP-43 aggregation.

Discussion

Most ALS and many FTD cases are characterised by TDP-43 aggregation [2, 41], which causes neurotoxicity through loss or gain of TDP-43 function [42-44]. Much research effort has been dedicated to determining whether aggregation of other proteins in ALS and FTD is similarly neurotoxic, or whether TDP-43 is the driver of neurodegeneration. The patterning of TDP-43 aggregate deposition in sporadic ALS, being most severe in the upper and lower motor neurons of the motor cortex and spinal cord, respectively, reflects the major symptomology as a paralysing motor disorder [6, 7]. Determining the patterning of other aggregating proteins with respect to neurodegeneration, symptomology, and the pattern of TDP-43 aggregation, could therefore reveal their relative contribution to disease. We mapped ubiquilin 2 and TDP-43 aggregates across the CNS in *UBQLN2*-linked ALS with or without FTD, finding that mutant ubiquilin 2 aggregates were abundant throughout much of the CNS; predominantly in different CNS subregions from TDP-43, or in the same subregion but different cells. The broad distribution of ubiquilin 2 aggregates in clinically unaffected regions in *UBQLN2*-linked cases supports the hypothesis that the aggregation of TDP-43 drives neurodegeneration more quickly or potently than that of ubiquilin 2. Contrastingly, the deposition of ubiquilin 2 aggregates in hippocampal sub-regions suggests that cognitive phenotypes may be strongly promoted by ubiquilin 2 aggregation.

Regional distribution of ubiquilin 2- and/or TDP-43-containing aggregates in *UBQLN2*-linked ALS/FTD

Regions of ubiquilin 2 aggregation described in previous studies of *UBQLN2*-linked ALS/FTD were spread across the CNS, including the neocortex, hippocampal formation, brain stem, and spinal cord [4, 10, 12, 13, 18, 20, 29]. Here we examined 40 brain subregions across the CNS, finding ubiquilin 2-only aggregates across the neocortex and enriched in layer VI of the motor cortex, in the dorsal and rarely the ventral horns of the spinal cord, in the molecular layer of the dentate gyrus of the hippocampus, the substantia nigra, and throughout the hippocampal-associated cortices, medulla, and striatum.

The vast majority of ubiquilin 2-only aggregates were punctate and neuritic or found in the neuropil, with larger diffuse aggregates detected mainly in the ventral striatum. Ubiquilin 2-only aggregates occasionally localised to MAP2-positive neurites and cell bodies. The majority of aggregates independent of MAP2-positive structures may have localised to astrocytes, microglia, or to MAP2-negative neuronal subtypes [45] or axons, given that MAP2 strongly labels dendrites but not axons [46, 47].

Of the regions we identified with aggregates of ubiquilin 2 in *UBQLN2*-linked ALS/FTD, the motor cortex, striatum, substantia nigra, and most subregions of the medulla had not previously been reported, while the hippocampal molecular layer had been reported in almost all previous studies. Notably, while the hippocampal molecular layer *did* show dense ubiquilin 2 aggregates in these cases, their density was 2-40x higher in the subiculum and perirhinal cortex. Compared to the hippocampal molecular layer, ubiquilin 2 aggregate density was also higher in the striatum and layer VI of the motor cortex. The focus upon the hippocampus as the major CNS region in which mutant ubiquilin 2 aggregates should therefore be reconsidered.

Is hippocampal ubiquilin 2 aggregation a determinant of frontotemporal dysfunction?

Overall, hippocampal ubiquilin 2-only aggregates were predominantly seen in *UBQLN2* p.T487I cases, and hippocampal TDP-43-only aggregates in stage 4 sALS cases, with a lack of regional relationship between the two proteins. The focus on hippocampal ubiquilin 2 aggregates in previous literature regarding *UBQLN2*-linked ALS/FTD may derive from their appearance also in *C9orf72*-linked ALS/FTD, but not in other forms of ALS [4, 48]. It is tempting to speculate that hippocampal ubiquilin 2 aggregates underpin the high frequency of co-morbid FTD in both *UBQLN2*-linked and *C9orf72*-linked cases [41, 49, 50]. FTD is characterised by neuronal loss beginning in the frontal and temporal lobes including the hippocampus, but progressing to involve most of the cortex and parts of the subcortex [51, 52]. The current finding of moderate-to-high deposition of ubiquilin 2 in the hippocampus in *UBQLN2*-linked ALS/FTD cases may suggest that hippocampal function is particularly vulnerable to gain or loss of function of ubiquilin 2.

It should be noted that hippocampal ubiquilin 2 aggregates in *UBQLN2*-linked ALS/FTD, seen in the dentate gyrus molecular layer, the subiculum, entorhinal cortex, and perirhinal cortex, were predominantly negative for TDP-43 as a 'seeding' protein. Our previous work found mutant ubiquilin 2 (as found in *UBQLN2*-linked cases) to be more aggregation-prone than wildtype ubiquilin 2 (as found in *C9orf72*-linked cases) [13]. In *UBQLN2*-linked cases, ubiquilin 2 aggregates in the granule cell dendrites that extend into the hippocampal molecular layer are labelled by the degradation adapter protein p62 and require no aggregation event in the granule cell soma. In contrast, in *C9orf72*-linked cases, ubiquilin 2 aggregates in the granule cell dendrites are not labelled by p62 and are associated with aggregation of dipeptide-repeat proteins (with or without TDP-43 and ubiquilin 2) in the granule cell soma. Thus, hippocampal molecular layer ubiquilin 2 aggregation in both genetic subtypes may report upon proteasomal inhibition (DPR-dependent [53, 54] or mutant ubiquilin 2-dependent [55]) in the granule cells but yield conformationally different products.

Similarly, ubiquilin 2 aggregates in the neurites extending into *other* hippocampal subregions may report upon the health of their cell-of-origin in a different subregion. Fibres from the perirhinal cortex extend into the lateral entorhinal cortex [56], and fibres from the entorhinal cortex extend towards and synapse with processes in the molecular layers of the subiculum and dentate gyrus, forming the perforant pathway [57]. There is evidence of perforant pathway damage in non-*UBQLN2*-linked ALS with FTD [57]. Therefore, in *UBQLN2*-linked ALS/FTD it is also possible that ubiquilin 2 aggregation 'spreads' from the perirhinal to entorhinal cortex, and along the perforant pathway to the subiculum and dentate gyrus molecular layer. The current work suggests that functional changes associated with ubiquilin 2 deposition may occur in cell types whose somata are distant from, but whose neurites project to, the site of aggregation.

Overall, ubiquilin 2 deposition appears to be associated with frontotemporal dysfunction, and that association does not depend on the co-deposition of TDP-43. Indeed, hippocampal deposition of TDP-43 (in the granule cells) is an *independent* determinant of

frontotemporal dysfunction, that may be seen in ~30% of cases of stage 4 sALS or *C9orf72*-linked ALS [6] or *UBQLN2*-linked ALS/FTD [13].

Is motor region ubiquilin 2 aggregation a determinant of motor dysfunction?

In both the spinal cord and motor cortex, ubiquilin 2-only aggregates were predominantly seen in *UBQLN2* p.T487I cases, while TDP-43-only aggregates were predominantly seen in stage 4 sALS cases, with a lack of regional relationship. TDP-43 aggregates were found in the somata of motor neurons known to degenerate in ALS/FTD [6, 7]; the Betz cells of layer Vb of the motor cortex and the lower motor neurons of layer IX of the ventral spinal cord. In contrast, ubiquilin 2-only aggregates were deposited in layer VI of the motor cortex and layer II of the dorsal horn of the spinal cord. So does ubiquilin 2 aggregation promote or act as a biomarker of motor dysfunction, or is it simply an epiphenomenon?

Motor cortex layer VI deposition of ubiquilin 2 is intriguing, given that the Betz cells are instead localised to the lower part of layer V, termed layer Vb [58]. Layer VI is the most complex of the cortical layers, containing a wide variety of neuronal cell types including excitatory pyramidal neurons that project dendrites and axons to layer V, establishing reciprocal connectivity [59-61]. However, ubiquilin 2-only aggregates in layer VI are punctate and co-localise frequently with MAP2-positive and occasionally with SMI-32-positive neurites, therefore are likely to be neuritic or localised to the neuropil rather than somatic. Analogous to the hippocampal molecular layer ubiquilin 2-only aggregates in neurites deriving from granule cell neurons, it may be that layer VI ubiquilin 2-only aggregates lie in neurites that derive from neurons elsewhere. Indeed, Betz cells themselves project dendrites to layer VI and may be the source of layer VI ubiquilin 2-only aggregates [58].

In the spinal cord, our findings were wholly unexpected. First, we detected abundant punctate ubiquilin 2-only aggregates in the dorsal horn in *UBQLN2*-linked ALS/FTD cases that were scarce in sALS. The dorsal horn relays sensory inputs, and is generally affected only subtly by ALS, if at all [62-65]. The pathomechanisms and consequences of

deposition of these aggregates warrant further investigation. Second, ubiquilin 2 has previously been shown to co-label TDP-43 aggregates in ventral horn lower motor neuron somata in *UBQLN2*-linked ALS/FTD cases and in sALS [4], yet we never saw this even with striking TDP-43 aggregate burden in the ventral horn and abundant ubiquilin 2-labelling in the dorsal horn. The antibody we used appears to be the same as that used by [4], based on the identical validation images and blots in the antibody datasheets (This study: mouse monoclonal anti-ubiquilin IgG2a, Santa Cruz #SC-100612; [4]: mouse monoclonal anti-ubiquilin IgG2a, clone 5F5, H00029978-M03 from Novus Biologicals). We have tested this antibody at a high concentration (2 µg/mL) as well as another ubiquilin 2 antibody (Novus Biologicals NBP2-25164) but we do not detect ubiquilin 2 co-labelling of TDP-43 aggregates in ventral horn in either *UBQLN2*-linked ALS/FTD cases or in sALS. If indeed ubiquilin 2 does not accumulate in ventral horn motor neurons, the main driver of lower motor neuron loss in *UBQLN2*-linked ALS may be deposition and dysfunction not of ubiquilin 2 but of TDP-43.

Unique ubiquilin 2 pathology in the striatum

The striatum was unusual for the abundance of larger diffuse ubiquilin 2 aggregates that had the globular appearance of neuronal cytoplasmic inclusions or aggresomes. We found previously that ubiquilin 2 decorates cytoplasmic inclusions or aggresomes of TDP-43 induced by autophagy and/or proteasome blockade *in vitro* [66], yet in *UBQLN2* p.T487I-linked ALS/FTD these inclusions were devoid of TDP-43. We hypothesise that only in the striatum does mutant ubiquilin 2 aggregate significantly in the cell soma, in contrast to its neuritic or neuropil aggregation elsewhere in the CNS.

Co-aggregation versus independent aggregation of ubiquilin 2

This brings us to our final discussion point, regarding the enhanced aggregation propensity of mutant compared to wildtype ubiquilin 2. This is indicated by i) the abundance of ubiquilin 2 aggregates in *UBQLN2* p.T487I cases compared even to stage 4 sALS cases with high TDP-43 aggregate loads; ii) the presence of ubiquilin 2 'aggresomes' only in p.T487I cases; and most notably, iii) the fact that nearly all ubiquilin 2 aggregates in *UBQLN2* p.T487I cases are negative for TDP-43 whereas rare

ubiquilin 2 aggregates in stage 4 sALS often incorporate TDP-43. We propose that TDP-43 drives the infrequent aggregation of wildtype ubiquilin 2 in sALS, while mutant ubiquilin 2 is intrinsically aggregation-prone and requires no driver.

Conclusion

Here we demonstrate that the ubiquilin 2 aggregates described in previous papers in *UBQLN2*-linked ALS/FTD are found across most of the CNS, where they are punctate in the neurites and neuropil. A unique population of larger diffuse aggresome-like ubiquilin 2 aggregates are also found in the striatum, but both punctate and diffuse ubiquilin 2 aggregates are generally negative for TDP-43. Therefore, while ubiquilin 2 aggregation may promote certain clinical features in *UBQLN2*-linked ALS/FTD, such as frontotemporal dementia, overall symptomology maps best to the aggregation of TDP-43.

List of abbreviations

ALS	Amyotrophic lateral sclerosis
C9orf72	Chromosome 9 open reading frame 72
CNS	Central nervous system
DPR	Dipeptide repeat
FFPE	Formalin-fixed paraffin-embedded
FTD	Frontotemporal dementia
PBS	Phosphate-buffered saline
pTDP-43	Phosphorylated TDP-43
sALS	Sporadic ALS
TDP-43	Transactive response DNA binding protein 43 kDa
UBQLN2	Ubiquilin 2 gene

Disclosures and declarations

Data transparency

The datasets used and/or analysed during the current study are available from the corresponding author on reasonable request.

Compliance with ethical standards

Conflicts of interest

The authors declare that they have no conflicts of interest.

Research involving human participants

All protocols were approved by the University of Auckland Human Participants Ethics Committee (New Zealand) and carried out as per approved guidelines. This study was also approved by the Human Research Ethics Committee of Macquarie University (520211013428875) and the Concord Hospital Research Ethics Committee.

Informed consent

Informed donor consent and ethical approvals were obtained at each site.

References

1. Arai, T., et al., *TDP-43 is a component of ubiquitin-positive tau-negative inclusions in frontotemporal lobar degeneration and amyotrophic lateral sclerosis.* Biochem Biophys Res Commun, 2006. **351**(3): p. 602-11.
2. Neumann, M., et al., *Ubiquitinated TDP-43 in frontotemporal lobar degeneration and amyotrophic lateral sclerosis.* Science, 2006. **314**(5796): p. 130-3.
3. Mackenzie, I.R., et al., *Pathological TDP-43 distinguishes sporadic amyotrophic lateral sclerosis from amyotrophic lateral sclerosis with SOD1 mutations.* Ann Neurol, 2007. **61**(5): p. 427-34.
4. Deng, H.X., et al., *Mutations in UBQLN2 cause dominant X-linked juvenile and adult-onset ALS and ALS/dementia.* Nature, 2011. **477**(7363): p. 211-5.
5. Mori, K., et al., *Bidirectional transcripts of the expanded C9orf72 hexanucleotide repeat are translated into aggregating dipeptide repeat proteins.* Acta Neuropathol, 2013. **126**(6): p. 881-93.
6. Brettschneider, J., et al., *Stages of pTDP-43 pathology in amyotrophic lateral sclerosis.* Ann Neurol, 2013. **74**(1): p. 20-38.
7. Brettschneider, J., et al., *TDP-43 pathology and neuronal loss in amyotrophic lateral sclerosis spinal cord.* Acta Neuropathol, 2014. **128**(3): p. 423-37.
8. Waters, S., et al., *Blood-spinal cord barrier leakage is independent of motor neuron pathology in ALS.* Acta Neuropathol Commun, 2021. **9**(1): p. 144.
9. Mackenzie, I.R., et al., *Dipeptide repeat protein pathology in C9ORF72 mutation cases: clinico-pathological correlations.* Acta Neuropathol, 2013. **126**(6): p. 859-79.
10. Gkazi, S.A., et al., *Striking phenotypic variation in a family with the P506S UBQLN2 mutation including amyotrophic lateral sclerosis, spastic paraplegia, and frontotemporal dementia.* Neurobiol Aging, 2018.
11. Scotter, E.L., et al., *C9ORF72 and UBQLN2 mutations are causes of amyotrophic lateral sclerosis in New Zealand: a genetic and pathologic study using banked human brain tissue.* Neurobiology of aging, 2017. **49**: p. 214. e1-214. e5.
12. Williams, K.L., et al., *UBQLN2/ubiquilin 2 mutation and pathology in familial amyotrophic lateral sclerosis.* Neurobiol Aging, 2012. **33**(10): p. 2527 e3-10.
13. Thumbadoo, K.M., et al., *Hippocampal protein aggregation signatures fully distinguish pathogenic and wildtype UBQLN2 in amyotrophic lateral sclerosis.* bioRxiv, 2022: p. 2022.01.12.475792.
14. Kleijnen, M.F., et al., *The hPLIC proteins may provide a link between the ubiquitination machinery and the proteasome.* Mol Cell, 2000. **6**(2): p. 409-19.
15. Walters, K.J., et al., *Structural studies of the interaction between ubiquitin family proteins and proteasome subunit S5a.* Biochemistry, 2002. **41**(6): p. 1767-77.
16. N'Diaye, E.N., J. Debnath, and E.J. Brown, *Ubiquilins accelerate autophagosome maturation and promote cell survival during nutrient starvation.* Autophagy, 2009. **5**(4): p. 573-5.
17. Osaka, M., et al., *Evidence of a link between ubiquilin 2 and optineurin in amyotrophic lateral sclerosis.* Hum Mol Genet, 2015. **24**(6): p. 1617-29.

18. Wu, J.J., et al., *ALS/FTD mutations in UBQLN2 impede autophagy by reducing autophagosome acidification through loss of function.* Proceedings of the National Academy of Sciences, 2020: p. 201917371.
19. Dao, T.P., et al., *Ubiquitin Modulates Liquid-Liquid Phase Separation of UBQLN2 via Disruption of Multivalent Interactions.* Mol Cell, 2018. **69**(6): p. 965-978 e6.
20. Fahed, A.C., et al., *UBQLN2 mutation causing heterogeneous X-linked dominant neurodegeneration.* Ann Neurol, 2014. **75**(5): p. 793-798.
21. Teyssou, E., et al., *Novel UBQLN2 mutations linked to amyotrophic lateral sclerosis and atypical hereditary spastic paraplegia phenotype through defective HSP70-mediated proteolysis.* Neurobiol Aging, 2017. **58**: p. 239 e11-239 e20.
22. Vengoechea, J., et al., *Clinical variability and female penetrance in X-linked familial FTD/ALS caused by a P506S mutation in UBQLN2.* Amyotroph Lateral Scler Frontotemporal Degener, 2013. **14**(7-8): p. 615-9.
23. Dao, T.P., et al., *ALS-Linked Mutations Affect UBQLN2 Oligomerization and Phase Separation in a Position- and Amino Acid-Dependent Manner.* Structure, 2019. **27**(6): p. 937-951 e5.
24. Ceballos-Diaz, C., et al., *Viral expression of ALS-linked ubiquilin-2 mutants causes inclusion pathology and behavioral deficits in mice.* Mol Neurodegener, 2015. **10**: p. 25.
25. Picher-Martel, V., et al., *Neuronal Expression of UBQLN2(P497H) Exacerbates TDP-43 Pathology in TDP-43(G348C) Mice through Interaction with Ubiquitin.* Mol Neurobiol, 2019. **56**(7): p. 4680-4696.
26. Buratti, E. and F.E. Baralle, *Characterization and functional implications of the RNA binding properties of nuclear factor TDP-43, a novel splicing regulator of CFTR exon 9.* J Biol Chem, 2001. **276**(39): p. 36337-43.
27. Polymenidou, M., et al., *Long pre-mRNA depletion and RNA missplicing contribute to neuronal vulnerability from loss of TDP-43.* Nat Neurosci, 2011. **14**(4): p. 459-68.
28. Hasegawa, M., et al., *Phosphorylated TDP-43 in frontotemporal lobar degeneration and amyotrophic lateral sclerosis.* Ann Neurol, 2008. **64**(1): p. 60-70.
29. Scotter, E.L., et al., *C9ORF72 and UBQLN2 mutations are causes of amyotrophic lateral sclerosis in New Zealand: a genetic and pathologic study using banked human brain tissue.* Neurobiol Aging, 2017. **49**: p. 214 e1-214 e5.
30. Waldvogel, H.J., et al., *The collection and processing of human brain tissue for research.* Cell Tissue Bank, 2008. **9**(3): p. 169-79.
31. Waldvogel, H.J., et al., *Immunohistochemical staining of post-mortem adult human brain sections.* Nat Protoc, 2006. **1**(6): p. 2719-32.
32. Murray, H.C., et al., *Lamina-specific immunohistochemical signatures in the olfactory bulb of healthy, Alzheimer's and Parkinson's disease patients.* Commun Biol, 2022. **5**(1): p. 88.
33. Maric, D., et al., *Whole-brain tissue mapping toolkit using large-scale highly multiplexed immunofluorescence imaging and deep neural networks.* Nat Commun, 2021. **12**(1): p. 1550.

34. Sternberger, L.A. and N.H. Sternberger, *Monoclonal antibodies distinguish phosphorylated and nonphosphorylated forms of neurofilaments in situ.* Proc Natl Acad Sci U S A, 1983. **80**(19): p. 6126-30.
35. Voelker, C.C., et al., *Selective neurofilament (SMI-32, FNP-7 and N200) expression in subpopulations of layer V pyramidal neurons in vivo and in vitro.* Cereb Cortex, 2004. **14**(11): p. 1276-86.
36. Flace, P., et al., *Calbindin-D28K immunoreactivity in the human cerebellar cortex.* Anat Rec (Hoboken), 2014. **297**(7): p. 1306-15.
37. Nag, T.C. and S. Wadhwa, *Calbindin immunoreactivity in the developing and adult human cerebellum.* J Chem Neuroanat, 1999. **17**(1): p. 1-12.
38. Haber, S.N. and S.J. Watson, *The comparative distribution of enkephalin, dynorphin and substance P in the human globus pallidus and basal forebrain.* Neuroscience, 1985. **14**(4): p. 1011-24.
39. Haber, S.N. and S.J. Watson, *The comparison between enkephalin-like and dynorphin-like immunoreactivity in both monkey and human globus pallidus and substantia nigra.* Life Sci, 1983. **33 Suppl 1**: p. 33-6.
40. Woolf, Z., et al., *Single-cell image analysis reveals a protective role for microglia in glioblastoma.* Neuro-Oncology Advances, 2021. **3**(1).
41. Ling, S.C., M. Polymenidou, and D.W. Cleveland, *Converging mechanisms in ALS and FTD: disrupted RNA and protein homeostasis.* Neuron, 2013. **79**(3): p. 416-38.
42. Lee, E.B., V.M. Lee, and J.Q. Trojanowski, *Gains or losses: molecular mechanisms of TDP43-mediated neurodegeneration.* Nat Rev Neurosci, 2011. **13**(1): p. 38-50.
43. Scotter, E.L., H.J. Chen, and C.E. Shaw, *TDP-43 Proteinopathy and ALS: Insights into Disease Mechanisms and Therapeutic Targets.* Neurotherapeutics, 2015. **12**(2): p. 352-63.
44. Keating, S.S., et al., *TDP-43 pathology: From noxious assembly to therapeutic removal.* Prog Neurobiol, 2022. **211**: p. 102229.
45. Chamak, B., et al., *MAP2 expression and neuritic outgrowth and branching are coregulated through region-specific neuro-astroglial interactions.* J Neurosci, 1987. **7**(10): p. 3163-70.
46. Dehmelt, L. and S. Halpain, *The MAP2/Tau family of microtubule-associated proteins.* Genome Biol, 2005. **6**(1): p. 204.
47. Caceres, A., et al., *Differential subcellular localization of tubulin and the microtubule-associated protein MAP2 in brain tissue as revealed by immunocytochemistry with monoclonal hybridoma antibodies.* J Neurosci, 1984. **4**(2): p. 394-410.
48. Brettschneider, J., et al., *Pattern of ubiquilin pathology in ALS and FTLD indicates presence of C9ORF72 hexanucleotide expansion.* Acta Neuropathol, 2012. **123**(6): p. 825-39.
49. Renton, A.E., A. Chio, and B.J. Traynor, *State of play in amyotrophic lateral sclerosis genetics.* Nat Neurosci, 2014. **17**(1): p. 17-23.
50. DeJesus-Hernandez, M., et al., *Expanded GGGGCC hexanucleotide repeat in noncoding region of C9ORF72 causes chromosome 9p-linked FTD and ALS.* Neuron, 2011. **72**(2): p. 245-56.

51. Broe, M., et al., *Staging disease severity in pathologically confirmed cases of frontotemporal dementia.* Neurology, 2003. **60**(6): p. 1005-11.
52. Kril, J.J. and G.M. Halliday, *Clinicopathological staging of frontotemporal dementia severity: correlation with regional atrophy.* Dement Geriatr Cogn Disord, 2004. **17**(4): p. 311-5.
53. Bozic, J., et al., *Interactome screening of C9orf72 dipeptide repeats reveals VCP sequestration and functional impairment by polyGA.* Brain, 2022. **145**(2): p. 684-699.
54. May, S., et al., *C9orf72 FTLD/ALS-associated Gly-Ala dipeptide repeat proteins cause neuronal toxicity and Unc119 sequestration.* Acta Neuropathol, 2014. **128**(4): p. 485-503.
55. Funakoshi, M., et al., *Budding yeast Dsk2p is a polyubiquitin-binding protein that can interact with the proteasome.* Proc Natl Acad Sci U S A, 2002. **99**(2): p. 745-50.
56. Suzuki, W.A. and Y. Naya, *The perirhinal cortex.* Annu Rev Neurosci, 2014. **37**: p. 39-53.
57. Takeda, T., et al., *Memory deficits in amyotrophic lateral sclerosis patients with dementia and degeneration of the perforant pathway A clinicopathological study.* J Neurol Sci, 2007. **260**(1-2): p. 225-30.
58. Braak, H. and E. Braak, *The pyramidal cells of Betz within the cingulate and precentral gigantopyramidal field in the human brain. A Golgi and pigmentarchitectonic study.* Cell Tissue Res, 1976. **172**(1): p. 103-19.
59. Zhang, Z.W. and M. Deschenes, *Intracortical axonal projections of lamina VI cells of the primary somatosensory cortex in the rat: a single-cell labeling study.* J Neurosci, 1997. **17**(16): p. 6365-79.
60. Thomson, A.M., *Neocortical layer 6, a review.* Front Neuroanat, 2010. **4**: p. 13.
61. Briggs, F., *Organizing principles of cortical layer 6.* Front Neural Circuits, 2010. **4**: p. 3.
62. Diaz, E. and H. Morales, *Spinal Cord Anatomy and Clinical Syndromes.* Semin Ultrasound CT MR, 2016. **37**(5): p. 360-71.
63. Isaacs, J.D., et al., *Amyotrophic lateral sclerosis with sensory neuropathy: part of a multisystem disorder?* J Neurol Neurosurg Psychiatry, 2007. **78**(7): p. 750-3.
64. Sabado, J., et al., *Accumulation of misfolded SOD1 in dorsal root ganglion degenerating proprioceptive sensory neurons of transgenic mice with amyotrophic lateral sclerosis.* Biomed Res Int, 2014. **2014**: p. 852163.
65. Tao, Q.Q., Q. Wei, and Z.Y. Wu, *Sensory nerve disturbance in amyotrophic lateral sclerosis.* Life Sci, 2018. **203**: p. 242-245.
66. Scotter, E.L., et al., *Differential roles of the ubiquitin proteasome system and autophagy in the clearance of soluble and aggregated TDP-43 species.* J Cell Sci, 2014. **127**(Pt 6): p. 1263-78.

Figure legends

Figure 1. Ubiquilin 2 and TDP-43 labelling in previous studies largely fails to discriminate between independent aggregation and co-aggregation

Schematic summary of literature describing ubiquilin 2 and TDP-43 neuropathology in *UBQLN2*-linked human ALS/FTD. Ubiquilin 2 aggregates (green box with plus) or TDP-43 aggregates (red box with plus) in each CNS region were either; not both tested (one plus or minus), not both identified (one plus, one minus), both identified but co-localisation not tested (dashed black box), or co-localised (shared black box). *Co-localisation in certain cases only. Abbreviations: ML, molecular layer; GCL, granule cell layer; PL, polymorphic layer; CA, cornu ammonis; PHG, parahippocampal gyrus; SC, spinal cord; MC, motor cortex; NCx, neocortex; Amg, amygdala; Put, putamen; Thal, thalamus; HN, hypoglossal nucleus ION, inferior olivary nucleus.

Figure 2. Morphology of ubiquilin 2 aggregates in *UBQLN2* p.T487I-linked ALS/FTD. Sections from across the CNS from representative *UBQLN2* p.T487I-linked ALS/FTD case V:7 (**A, B, D, F**) and representative stage 4 sALS case MN30 (**C, E, G**). *UBQLN2* p.T487I-linked ALS/FTD cases harboured many small punctate ubiquilin 2 aggregates (green, $\mathbf{A_1}$, caudate nucleus) and few large diffuse ubiquilin 2 aggregates (green, $\mathbf{A_2}$, caudate nucleus). Spinal cord ventral horn motor neurons demonstrated large TDP-43 aggregates (red) that were negative for ubiquilin 2 (green) in both *UBQLN2* p.T487I-linked ALS/FTD (**B**) and stage 4 sALS (**C**). Dorsal horn demonstrated small punctate ubiquilin 2 aggregates (green) that were negative for TDP-43 (red) in *UBQLN2* p.T487I-linked ALS/FTD (**D**) and in stage 4 sALS where they were smaller and dot-like (**E**). Motor cortex demonstrated TDP-43 aggregates (red) that were negative for ubiquilin 2 (green) in both *UBQLN2* p.T487I-linked ALS/FTD (**F”**) and stage 4 sALS (**G”**); and small punctate ubiquilin 2 aggregates (green) that were negative for TDP-43 (red) in *UBQLN2* p.T487I-linked ALS/FTD (**F’**) and in stage 4 sALS where they were dot-like (**G**). Scale bar in images A and B-F 20 µm; in A_1 and A_2 5 µm.

Figure 3. Ubiquilin 2-only and TDP-43-only aggregates in the *UBQLN2* p.T487I-linked ALS/FTD hippocampal formation, and entorhinal and perirhinal cortices.

Hippocampal sections from 2 *UBQLN2* p.T487I-linked ALS/FTD cases (**A-J”**) demonstrated punctate aggregates in the dentate gyrus molecular layer (**A_1, B_1**) that were positive for ubiquilin 2 only (**A_1’, B’$_1$,** green) and negative for TDP-43 (**A_1”, B_1”**). Case V:7 showed rare granule cell layer cytoplasmic aggregates of TDP-43 only (**B_2”,** red) that were negative for ubiquilin 2 (**B_2’**). Cornu ammonis and parahippocampal subregions showed abundant punctate ubiquilin 2-only aggregates (**C’-J’**) and fewer TDP-43-only aggregates (**C”-J”**) that were each negative for the other protein. Quantification of the density of ubiquilin 2-only (green) and TDP-43-only (red) aggregates showed that in *UBQLN2* p.T487I-linked ALS/FTD cases both aggregate types were highest in subiculum (**K**), while in stage 4 sALS ubiquilin 2-only aggregates were rare or absent but TDP-43-only aggregates were found throughout the hippocampal formation, particularly in the granule cell layer (**L**). Scale bars in A, B, 100 µm; others 20 µm. Abbreviations: ML, molecular layer; GCL, granule cell layer; PL, polymorphic layer; CA, cornu ammonis; Sub, subiculum; EC, entorhinal cortex; PC, piriform cortex.

Figure 4. Ubiquilin 2-only and TDP-43-only aggregates in the *UBQLN2* p.T487I-linked ALS/FTD spinal cord.

Spinal cord sections from 3 *UBQLN2* p.T487I-linked ALS/FTD cases (**A-F_1”**) demonstrated punctate aggregates in the dorsal horn (**A, B, C**) that were positive for ubiquilin 2 only (**A_1’, B_1’, C_1’,** green) and negative for TDP-43 (**A_1”, B_1”, C_1”**). The ventral horns showed abundant cytoplasmic and neuropil TDP-43-only aggregates (**D_1”, E_1”, F_1”,** red) that were negative for ubiquilin 2 (**D_1’, E_1’, F_1’**). Quantification of the density of aggregates confirmed that in *UBQLN2* p.T487I-linked ALS/FTD cases ubiquilin 2-only aggregates (green) were most abundant in the dorsal horn but TDP-43-only aggregates (red) were most abundant in the ventral horn (highlighted by pale red shading) (**G**). The same pattern was observed in stage 4 sALS cases but with only rare ubiquilin 2-only aggregates in the dorsal horn (**H**). Scale bar in main images, 200 µm; in insets 20 µm. Abbreviations: VWM, ventral white matter; VGM, ventral grey matter; DGM, dorsal grey matter; DWM, dorsal white matter.

Figure 5. Ubiquilin 2-only and TDP-43-only aggregates in the *UBQLN2* p.T487I-linked ALS/FTD motor cortex.

Motor cortex sections from 3 *UBQLN2* p.T487I-linked ALS/FTD cases (**A-C$_5$**) demonstrated aggregates in the cortical layers I-VI that were positive for ubiquilin 2 only (green) or TDP-43 only (red), but rarely positive for both (**A$_1$-A$_5$, B$_1$-B$_5$, C$_1$-C$_5$**). Quantification of the density of aggregates demonstrated that in *UBQLN2* p.T487I-linked ALS/FTD cases ubiquilin 2-only aggregates (green) were most abundant in layer VI, but TDP-43-only aggregates (red) were found throughout the cortical layers with case IV:10 showing higher density in layers III and V (highlighted by pale red shading) (**D**). Stage 4 sALS cases showed very rare ubiquilin 2-only aggregates but TDP-43-only aggregates were found throughout the cortical layers (**E**). Scale bar in main images, 200 µm; in insets 20 µm. Abbreviations: GM, grey matter; WM, white matter.

Figure 6. Ubiquilin 2-only and TDP-43-only aggregates in the *UBQLN2* p.T487I-linked ALS/FTD striatum.

Striatal sections from 2 *UBQLN2* p.T487I-linked ALS/FTD cases demonstrated abundant punctate and some large diffuse aggregates in the putamen, caudate nucleus, and ventral striatum, that were positive for ubiquilin 2 only and negative for TDP-43 (**A-E$_2$**, green). TDP-43-only aggregates were also present in these subregions but were less abundant (**A-E$_2$**, red). Quantification of the density of aggregates confirmed that in *UBQLN2* p.T487I-linked ALS/FTD cases ubiquilin 2-only aggregates (green) were more abundant than TDP-43-only aggregates (red) (**F**). Stage 4 sALS case MN30 showed deposition of ubiquilin 2-only aggregates in putamen and ventral striatum, while case MN15 showed particularly abundant TDP-43-only aggregates across the striatum (**G**). Scale bar in main images, 100 µm; in insets 20 µm. Abbreviations: CN, caudate nucleus; Put, putamen; VS, ventral striatum.

Study	Hippocampal formation												
	ML	GCL	PL	CA	PHG	SC	MC	NCx	Amg	Put	Thal	HN	ION
Deng et al., 2011	+ −	−		+		+ +							
Williams et al., 2012						+ +							
Fahed et al., 2014	+	−											+
Scotter et al., 2017	+	−			+		+						
Gkazi et al., 2019	+	+ +						+ +	+	+	+	+	
Wu et al., 2020	+	−	−										
Thumbadoo et al., 2022	+ −	+ + *											

Key

- Ubiquilin 2
- p-TDP-43
- Co-localisation
- Co-localisation possible but not examined
- + Presence of pathology
- − Absence of pathology

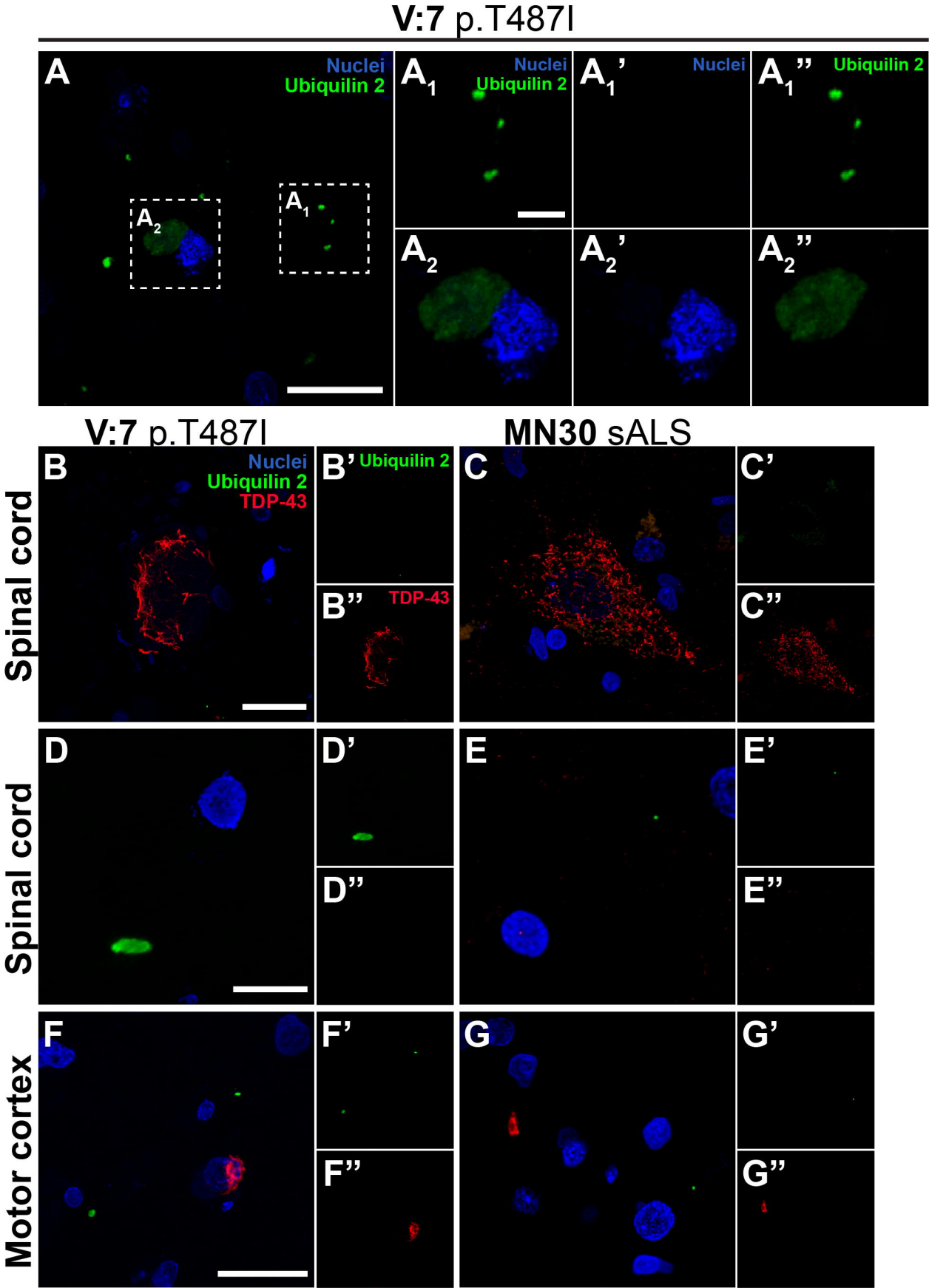
V:7 p.T487I
A
Nuclei
Ubiquilin 2
A2
A1
A1
Nuclei
Ubiquilin 2
A1'
Nuclei
A1''
Ubiquilin 2
A2
A2'
A2''
V:7 p.T487I
MN30 sALS
Spinal cord
B
Nuclei
Ubiquilin 2
TDP-43
B' Ubiquilin 2
B''
TDP-43
C
C'
C''
Spinal cord
D
D'
D''
E
E'
E''
Motor cortex
F
F'
F''
G
G'
G''

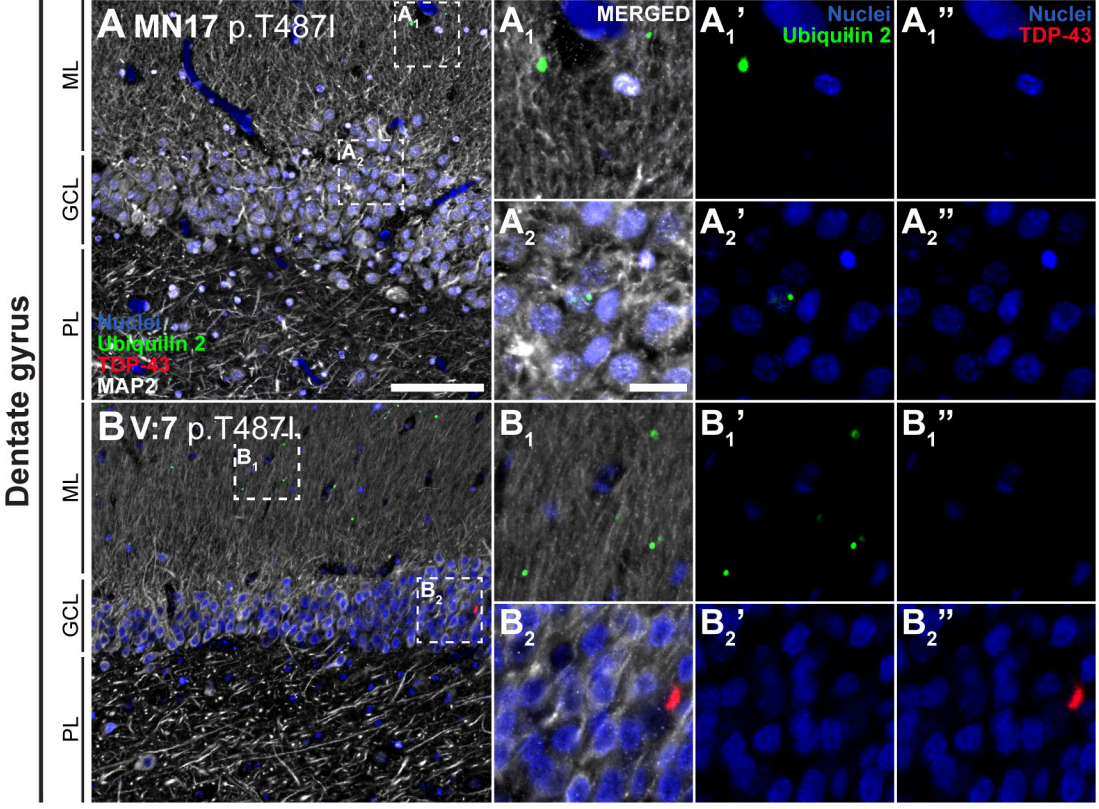
A MN17 p.T487I
MERGED
Nuclei
Ubiquilin 2
TDP-43
MAP2
B V:7 p.T487I
Dentate gyrus
ML
GCL
PL

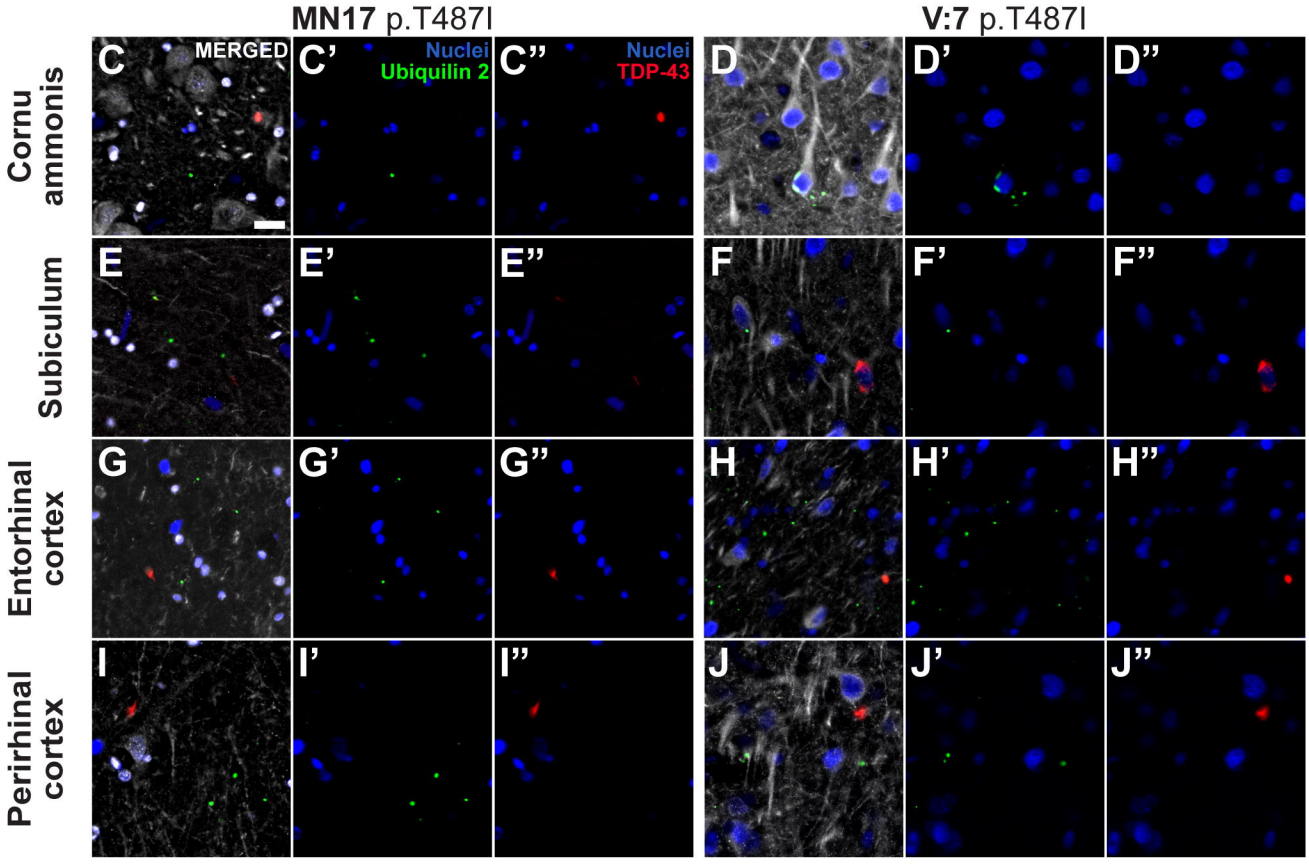
MN17 p.T487I
V:7 p.T487I
MERGED
Nuclei
Ubiquilin 2
TDP-43
Cornu ammonis
Subiculum
Entorhinal cortex
Perirhinal cortex

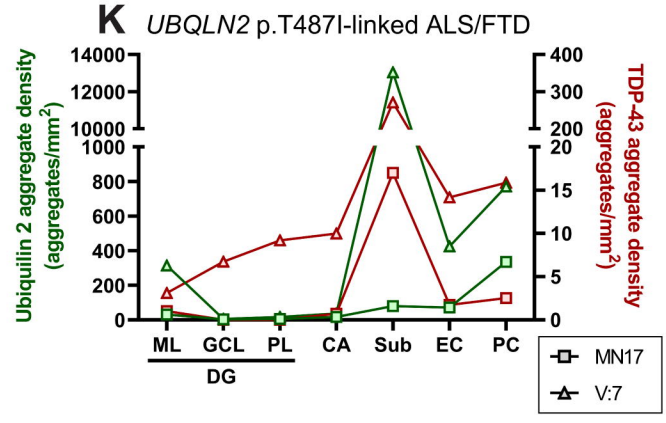
K UBQLN2 p.T487I-linked ALS/FTD
Ubiquilin 2 aggregate density (aggregates/mm2)
TDP-43 aggregate density (aggregates/mm2)
ML
GCL
PL
CA
Sub
EC
PC
DG
MN17
V:7

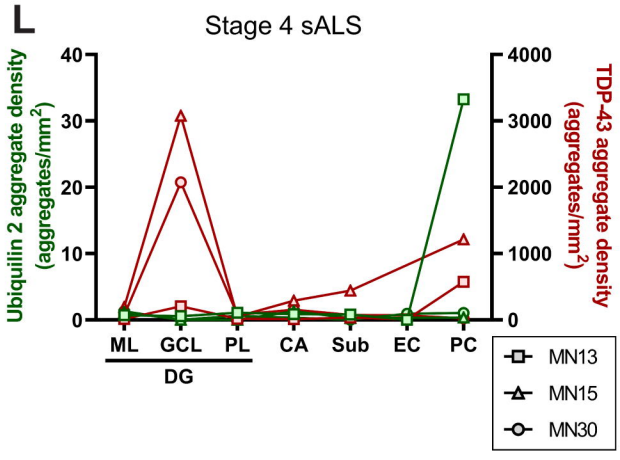
L Stage 4 sALS
Ubiquilin 2 aggregate density (aggregates/mm2)
TDP-43 aggregate density (aggregates/mm2)
ML
GCL
PL
CA
Sub
EC
PC
DG
MN13
MN15
MN30

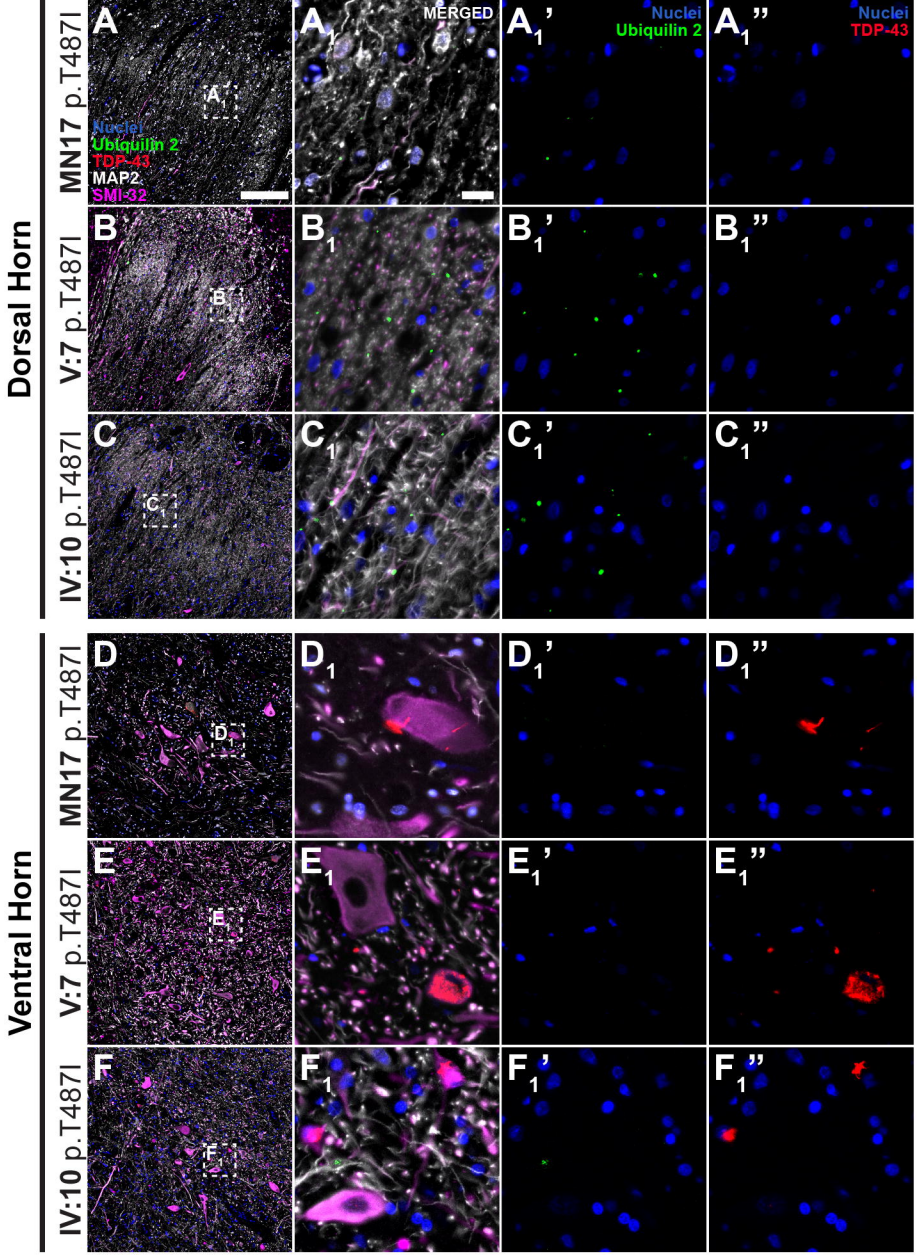
Dorsal Horn
Ventral Horn
MN17 p.T487I
V:7 p.T487I
IV:10 p.T487I
Nuclei
Ubiquilin 2
TDP-43
MAP2
SMI-32
MERGED
A
B
C
D
E
F

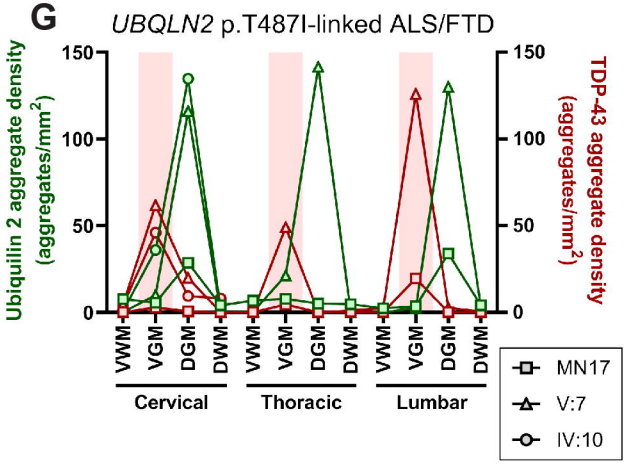
G
UBQLN2 p.T487I-linked ALS/FTD
Ubiquilin 2 aggregate density (aggregates/mm2)
TDP-43 aggregate density (aggregates/mm2)
VWM
VGM
DGM
DWM
Cervical
Thoracic
Lumbar
MN17
V:7
IV:10

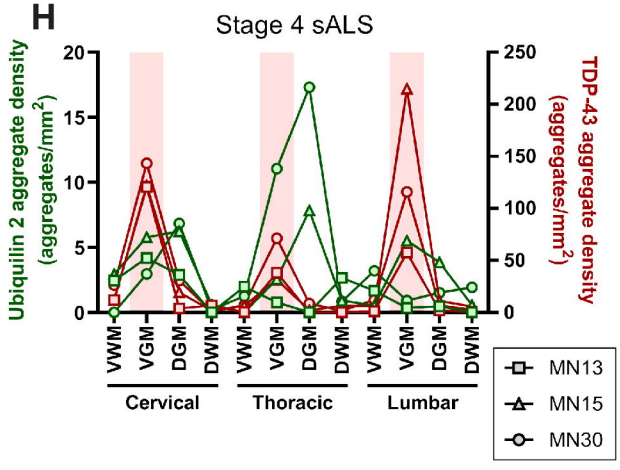
H
Stage 4 sALS
Ubiquilin 2 aggregate density (aggregates/mm2)
TDP-43 aggregate density (aggregates/mm2)
VWM
VGM
DGM
DWM
Cervical
Thoracic
Lumbar
MN13
MN15
MN30

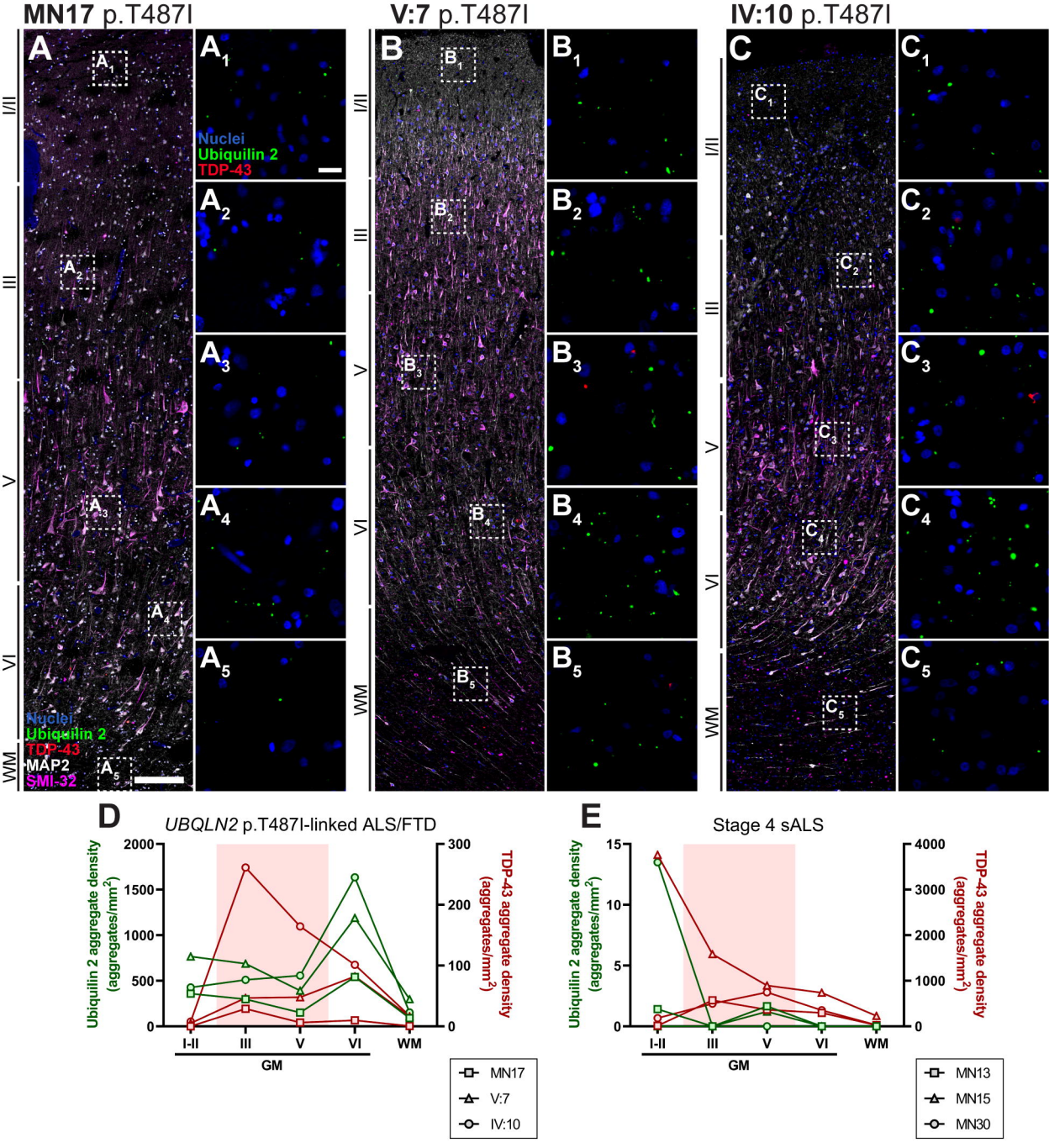
MN17 p.T487I
V:7 p.T487I
IV:10 p.T487I
A
B
C
I/II
III
V
VI
WM
Nuclei
Ubiquilin 2
TDP-43
MAP2
SMI-32
D
UBQLN2 p.T487I-linked ALS/FTD
Ubiquilin 2 aggregate density (aggregates/mm2)
TDP-43 aggregate density (aggregates/mm2)
GM
MN17
V:7
IV:10
E
Stage 4 sALS
MN13
MN15
MN30

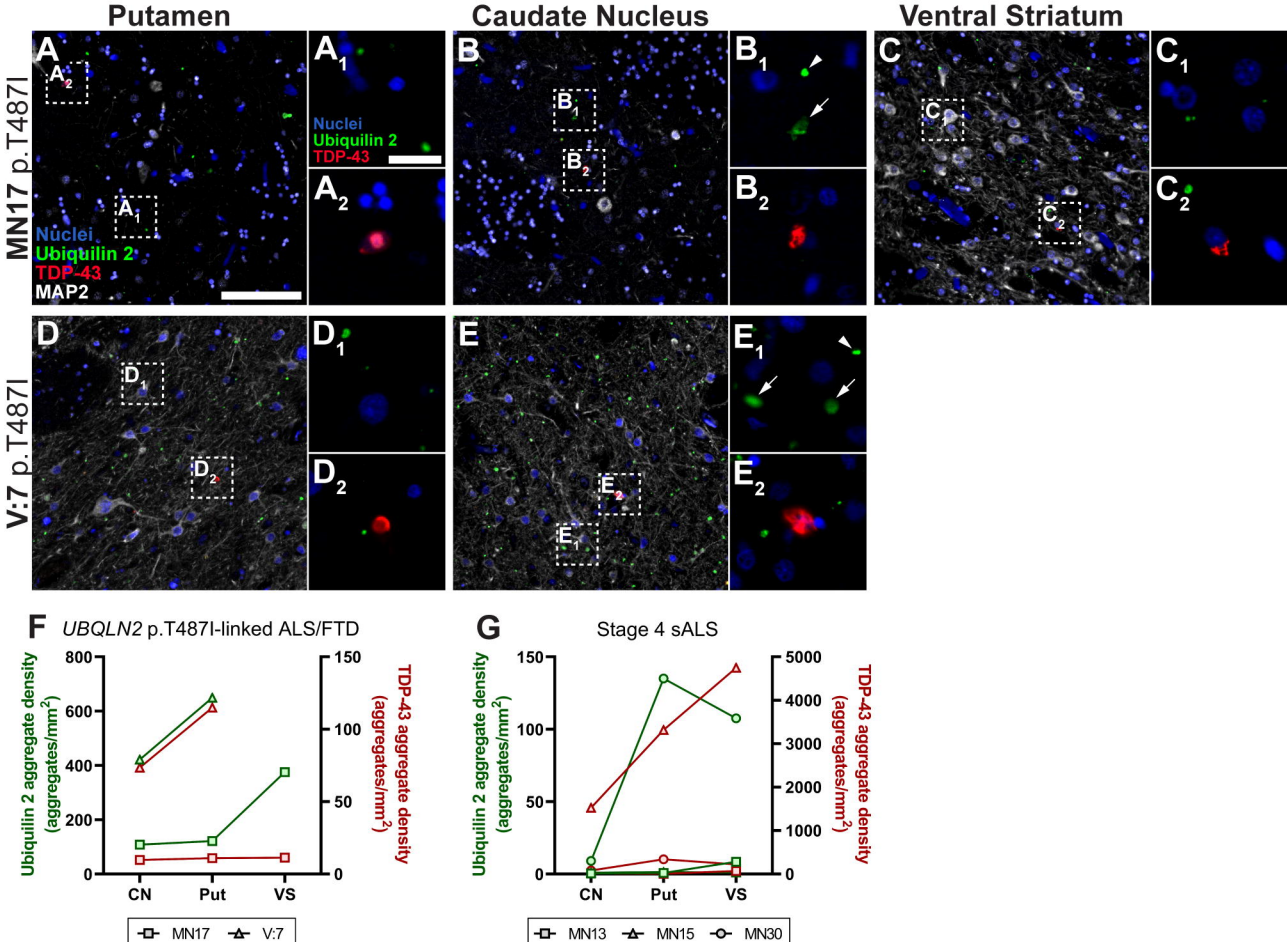
Putamen
Caudate Nucleus
Ventral Striatum
MN17 p.T487I
V:7 p.T487I
Nuclei
Ubiquilin 2
TDP-43
MAP2
F
UBQLN2 p.T487I-linked ALS/FTD
Ubiquilin 2 aggregate density (aggregates/mm2)
TDP-43 aggregate density (aggregates/mm2)
CN
Put
VS
MN17
V:7
G
Stage 4 sALS
MN13
MN15
MN30